Original Research Paper

Dual-responsive nanovaccine for cytosolic delivery of antigens to boost cellular immune responses and cancer immunotherapy

Yang Sui [a,1], Ji Li [b,1], Jiqiang Qu [d], Ting Fang [e], Hongyan Zhang [f], Jian Zhang [a], Zheran Wang [c,*], Mingyu Xia [d,*], Yinghui Dai [b,*], Dongkai Wang [a,*]

[a] Department of Pharmaceutics, Shenyang Pharmaceutical University, Shenyang 110016, China
[b] Department of Traditional Chinese Medicine, Shenyang Pharmaceutical University, Shenyang 110016, China
[c] Department of Mathematics and Statistics, Auburn University, Auburn, AL 36849, USA
[d] School of Life Science and Biopharmaceutics, Shenyang Pharmaceutical University, Shenyang 110016, China
[e] School of Pharmacy, China Medical University, Shenyang 110122, China
[f] School of Pharmaceutical Sciences, Zhejiang Chinese Medical University, Hangzhou 310053, China

ARTICLE INFO

ABSTRACT

Cancer vaccine contributing to the success of the treatment and prevention of tumors has attracted a huge attention as a strategy for tumor immunotherapy in recent years. A major challenge of cancer vaccine is to target cytosols of dendritic cells (DCs) in the lymph nodes (LNs) to enhance efficiency of antigen cross-presentation, which elicits high levels of cytotoxic T-lymphocytes to destruct tumor cells. Here, we address this issue by conjugating ovalbumin (OVA) to PEG-PCL using disulfide bond (-ss-), and the degradable pH-responsive polymer-PEI-PCL as delivery carrier. In addition, the mol ratio of PEG-PCL to PEI-PCL in the mixed micelles was tailored to deliver the OVA to LNs. Subsequently, CpG ODN$_{1826}$, a TLR-9 agonist, was further introduced into a mixed micelle of 30 nm or less as a unique tumor vaccine. Importantly, the results demonstrated the mixed micelles with 1:1 mol of PCL-PEG and PCL-PEI can effectively migrate to distal LNs where antigen were efficiently captured by DCs, meanwhile, OVA was modified to the surface of mixed micelles via disulfide bonds (-ss-) for promotion efficiency of antigen cross-presentation. More surprisingly, combination of tumor vaccine with anti-PD-1, the therapy of ectopic melanoma (B16-OVA) and lung metastasis melanoma (B16-OVA) is excellent therapeutic effect. Taken together, our works offers a novel strategy for the cytosol delivery of antigens to achieve potent cancer immunotherapy.

© 2022 Published by Elsevier B.V. on behalf of Shenyang Pharmaceutical University. This is an open access article under the CC BY-NC-ND license (http://creativecommons.org/licenses/by-nc-nd/4.0/)

---

* Corresponding authors.
E-mail addresses: zzw0049@auburn.edu (Z.R. Wang), xmywd@vip.sina.com (M.Y. Xia), yhdai2008@aliyun.com (Y.H. Dai), wangycsyphu@126.com (D.K. Wang).
[1] These authors contributed equally to the work.

1. Introduction

It is well known that cancer immunotherapy is to elicit a robust antigen-specific immune response to fight against cancer cells rather than directly attack tumor cells [1,2]. The cancer immunotherapies involving tumor vaccination [3], immune checkpoint blockade [4,5] and chimeric antigen receptor T-cell (CAR-T) [6] immunotherapy have been widely used for clinical trials [7–10]. Among these cancer immunotherapeutic approaches, cancer vaccines have been extensively researched because of relatively less expensiveness and low side effects [11–13]. However, the clinical efficacy has been is not satisfactory because the vaccine delivery system primarily induced the humoral immune response rather than the cellular immune responses, which are considered to be essential for the effectiveness of cancer vaccine [13,14]. Therefore, it is critical for developing a new nanoparticle-based vaccine delivery system that can maximize immunogenicity to improve the desired cellular immune response.

A major challenge of nanovaccine delivery systems is to target the cytosol of antigen-presenting cells (APCs), such as macrophages and DCs, as cellular immune response is determined by efficiency of MHC-I antigen cross-presentation (antigen peptide enter to the cytosol with major histocompatibility complex class I (MHC-I) form antigen peptide-MHC-I complexes, then antigen peptide-MHC-I interacts with CTLs), initiating of cellular immune responses to destruct tumor cells [15–18]. Nanoparticles (NPs) physico-chemical characteristics remarkably influenced the efficiency of antigen cross-presentation, including as size [19], surface modifications [20–22], and charge [8]. For example, NPs with sizes ranging from 10 to 100 nm were easier drained directly into LNs than large size NPs [19,23]. PEGylation of NPs is also a modality to enhance delivery to LNs and reduce retention at the injection site [22,24,25], since the PEG coating is able to reduce the interaction of NPs with glycosaminoglycans and collagen fibres in the interstitium, but it inhibits the uptake by DCs [23]. Previous studies indicated that positively charged NPs can facilitate the uptake by DCs more than negative or neutral charge [8], nevertheless, it increases the risk of NPs being trapped in the interstitium before reaching LNs [26,27]. In addition, one of the features of MHC-I presentation pathway is that antigens are mostly degraded in the cytosol, in which form complexes with MHC-I and then trigger cellular immune responses [28,29]. However, exogenous antigens are degraded in lysosomes, leading to MHC-II presentation, triggering humoral immune response [30,31]. Therefore, developing new vaccine vehicles to simultaneously maximize targeting DCs in LNs and cytosolic delivery of antigens can be challenging.

To resolve these challenges, combination of PCL-PEG with PCL-PEI was constructed the mixed micelles (denoted as PP) via modulating the mol ratio of two copolymers [32]. It is hoped to develop its respective advantages while evading its disadvantages in order that maximize LNs targeting and uptake by DCs. Polyethylenimine (PEI) is extensively employed as a gene delivery vector the tertiary, moreover, amine on the branched-PEI can be protonated under endo/lysosomal pH, which makes it has endo/lysosomal escape capacity [33,34,8]. PCL-PEG is widely used as a small hydrophobic drug delivery carrier [33], the PEG on the PCL-PEG backbone has the ability to reduce the reticuloendothelial system (RES) identification and intake, which makes it prolong the time of systemic circulation, and increase the half period [24]. In addition, we could utilize the feature of cytoplasmic reductive environment to conjugate antigens to the surface of NPs by a disulfide bond (-ss-), which is able to achieve cytosolic delivery of cargos, and boost efficiency of antigen cross-presentation [30,35,36]. Sachiko Hirosue ea tl. has revealed that reducible bond favored cytosolic delivery of antigens, to enhance antigen cross-presentation and generate cellular immune response [30].

In this work, we designed an intelligent scheme to conjugate OVA to the NPs surface by disulfide bond (denoted as PP-SS-OVA) in order that cytosolic delivery of antigens, triggering antigen-specific immune response. It is found that PP-SS-OVA has the ability to facilitate antigen MHC-I cross-presentation and DCs maturation, compared with OVA or nanovaccine by OVA and PP conjugated with amide bond. Thereafter, we further introduced CpG ODN_{1826}, a TLR-9 agonist [37], into PP-SS-OVA to generate PP-SS-OVA/CpG NPs. Surprisingly, PP-SS-OVA/CpG NPs as therapeutic vaccines could introduced high levels of antigen-specific CTLs activity that remarkably suppressed the growth of ectopic melanoma (B16-OVA) and lung metastasis melanoma (B16-OVA). In the further, combination of PP-SS-OVA/CpG with anti-PD1 immunotherapy could suppressed already-established ectopic melanoma and lung metastasis melanoma with significant immunotherapeutic effect. Therefore, our study has shown that PP-SS-OVA/CpG NPs was able to trigger excellent cellular immune response, meanwhile, the combination of PP-SS-OVA/CpG NPs with anti-PD1 provided an attractive combinational immunotherapy strategy for cancer treatment.

2. Materials and methods

2.1. Materials

Stannous octoate $(Sn(Oct)_2)$, polyethyleneimine (PEI), ε-caprolactone, 4-nitrophenyl chloroformate (NPC), N-(3-dimethylaminopropyl)-N'-ethylcarbodiimide (EDC), cysteamine hydrochloride, 2,2'-Dithiodipyridine, N-hydroxysuccinimide (NHS) were obtained from Aladdin (China). CpG ODN_{1826} and traut's reagent were obtained from Sangon Biotech (Shanghai). $HOOC-PEG-NH_2$ were purchased from Ponsure Biological (Shanghai). Carboxyfluorescein succinimidyl ester (CFSE), OVA, $OVA_{257-264}$, and $OVA_{323-339}$ were purchased from Sigma-Aldrich (USA). LysoTracker Red and DAPI were purchased from Beijing Solarbio Science & Technology Co.,Ltd. The anti-SIINFEKL/H-2K^{b}PE, anti-CD11c-BB700, anti-CD86-PE, anti-CD80-FITC, anti-CD3e-FITC, anti-CD4-APC and anti-CD8a-PerCP-Cy5.5 were obtained BD Biosciences (USA). IL-12p70, TNF-α and IFN-γ enzyme-linked immunosorbent assay (ELISA) kits were purchased from Invitrogen (USA). FITC–OVA was prepared according to the previous protocol.

2.2. Cells and animals

Female C57BL/6 and BALB/c mice aged six to eight weeks were obtained from the Laboratory Animal Center of Shenyang Pharmaceutical (Liaoning, China). B16-OVA melanoma cell was kindly provided by Prof. Siqing Wang (Jilin University, China). The BMDCs was prepared according to the previous protocol.

2.3. Synthesis and characterization of PCL-PEG and PCL-PEI copolymers

The synthesis procedures and characterization of different copolymers were presented in the Supporting Information.

2.4. Preparation and characterization of mixed micelles

Mixed micelles were prepared employing the conventional thin-film hydration procedure that had been prepared employing the under mol ratios of PEI-PCL to PEG-PCL 0:100 (PP0), 25:75 (PP25), 50:50 (PP50), 75:25 (PP75) and 100:0 (PP100). The particle size, ζ-potential and size distribution of micelles were analyzed by DLS. The critical micelle concentration (CMC) of micelles was analyzed by pyrene as a probe with fluorescence spectrophotometry.

2.5. Biodistribution of micelles-DiR in vivo

Female BALB/c mice were subcutaneously injected in the forepaw with Blank NPs, PP0, PP25, PP50, PP75 and PP100 (20 mg) containing DiR (1000 ng), and the mice were observed at 6 h, 24 h and 7 d employing IVIS spectrum (FX PRO, Carestream Health, Toronto, Canada). In a separate experiment, Female C57BL/6 mice were treated similarly procedure and were sacrificed at 24hr, and major organs were obtained respectively: heart, spleen, kidney, lung, liver and LNs. The LNs were analyzed by IVIS spectrum. LNs suspensions stained with anti-CD11c were analyzed by flow cytometry (FCM).

2.6. Preparation and characterization of PP-OVA, PP-SS-OVA and PP-SS-OVA/CPG

OVA-SH was prepared by reacting OVA with a 20 molar excess of Traut's reagent in PBS (5 ml, pH 7.8) at 4 °C for three days and then filtered. PP-SS-OVA$_{257-264}$ was prepared by a disulfide exchange reacting PDS groups on PP with HS-OVA$_{257-264}$ in PBS (5 mL, pH 7.4) at 4 °C for 24 h. As shown in Fig. 2A, PP-SS-OVA was prepared by a disulfide exchange reacting PDS groups on PP with OVA-SH in PBS (5 ml, pH 7.4) at 4 °C for 24 h. PP-OVA was prepared by reacting PP with OVA-NH$_2$ in the PBS (pH 7.4, 5 ml) for 24 h at 4 °C. The reducibility of the disulfide bond in the presence of 10 mM glutathione was observed via nonreducing SDS polyacrylamide gel electrophoresis (SDS-PAGE). PP-SS-OVA/CpG were formed by combining conjugates and CpG ODN$_{1826}$ at 25 °C for 30 min. CpG ODN$_{1826}$ was analyzed by a 2% agarose gel retardation assay. The ζ-potential and particle size of PP-OVA, PP-SS-OVA and PP-SS-OVA/CpG were analyzed employing Zetasizer Nano series. The surface morphology of PP-SS-OVA/CpG were investigated by transmission electrostatic microscopy (TEM, TecnaiG220, FEI, USA).

$$Conjugation\ Efficiency(\%) = (the\ conjugation\ of\ OVA)$$
$$/(the\ total\ of\ OVA) \times 100\%$$

$$Adsorption\ Efficiency(\%) = (the\ adsorption\ of\ CpG)$$
$$/(the\ total\ of\ CpG) \times 100\%$$

2.7. In vitro cellular cytotoxicity assay

Bone marrow-derived dendritic cells (BMDCs) were incubated with different formulations at a concentration gradient for 24 h. The cellular cytotoxicity of different formulations was then measured by standard thiazolyl tetrazolium (MTT) assay.

2.8. Intracellular uptake and localization of antigen assay in vitro

The cellular uptake of nanoparticle carriers was observed by Confocal laser scanning microscopy (CLSM).

For FCM assay, immature BMDCs were incubated with Blank, OVA, PP-OVA, PP-SS-OVA at 37 °C for 4 h. BMDCs were then harvested for analysis using FCM. For CLSM assay, immature BMDCs were incubated with Blank, OVA, PP-OVA, PP-SS-OVA at 37 °C for 4 h. BMDCs were fixed with 4% paraformaldehyde for 30 min. BMDCs were stained with DAPI, and then observed using CLSM.

CLSM were used to investigate the endosome/lysosome escape of nanoparticle carriers. For CLSM assay, immature BMDCs (2×10^5 cells/well) were incubated with Blank, OVA, PP-OVA, PP-SS-OVA for 1 or 4 h. BMDCs were stained with Lyso-Tracker^{TM} Red at 37 °C for 30 min. The cells were fixed with 4% paraformaldehyde for 30 min. BMDCs were stained with DAPI, and then observed using CLSM.

2.9. BMDCs cross-presentation assay in vitro

BMDCs (10^6/ml) were incubated in a 6-well plate with Blank NPs, PP-SS-OVA$_{257-264}$, PP-SS-OVA and PP-OVA for 24 h. BMDCs were incubated with anti-SIINFEKL/H-2K^{b}PE and anti-CD11c-BB700 for 30 min. The BMDCs were analyzed by FCM.

BMDCs (10^6/ml) were incubated in a 6-well plate with Blank, OVA, OVA+CpG, PP-OVA, PP-SS-OVA and PP-SS-OVA/CpG for 24 h. BMDCs were incubated with anti-SIINFEKL/H-2K^{b}PE and anti-CD11c-BB700 for 30 min. The BMDCs were analyzed by FCM.

2.10. BMDCs maturation assay in vitro

BMDCs (10^6/ml) were incubated in a 6-well plate with Blank, OVA, OVA+CpG, PP-OVA, PP-SS-OVA and PP-SS-OVA/CpG for 24 h. BMDCs were incubated with anti-CD11c-BB700, anti-CD80-FITC and anti-CD86-PE for 30 min. The BMDCs were measured by FCM. The cells supernatant was analyzed for TNF-α and IL-12p70 using ELISA.

2.11. DC maturation assay in vivo

Female C57BL/6 mice were subcutaneously immunized with Blank NPs, OVA, OVA+CpG, PP-OVA, PP-SS-OVA and PP-SS-

OVA/CpG. Seven days later, the lymph nodes from vaccinated mice were removed and mechanically disruption, meanwhile, digested into cell suspensions at 37 °C for 30 min in RPMI-1640 (collagenase IV, collagenase I, and hyaluronidase,). Cell suspension was then filtered to recover single cell suspension. The cell suspensions were incubated with anti-CD11c-BB700, anti-CD80-FITC and anti-CD86-PE for 30 min. The cell suspension was analyzed by FCM.

2.12. *In vivo CTLs assay*

Female C57BL/6 mice were subcutaneously immunized with Blank, OVA, OVA+CpG, PP-OVA, PP-SS-OVA and PP-SS-OVA/CpG. Seven days later, splenocytes were collected from spleens the naïve mice. Splenocytes were divided into two aliquots. One was pulsed in the presence of $OVA_{257-264}$ and the other in the presence of RPMI-1640 medium at 37 °C for 2 h. The $OVA_{257-264}$ part was stained with 5 mM CFSE ($CFSE_{high}$), while the RPMI-1640 complete medium part was stained with 0.5 mM CFSE ($CFSE_{low}$). Equal numbers of $CFSE_{high}$ (5×10^7 cells per ml) and $CFSE_{low}$ (5×10^7 cells per ml) were merged and injected intravenously into each experimental group. After 18 h, splenocytes were collected and measured by FCM.

$$Specific\,Lysis\,(\%) = \left[1 - \left(ratio\,of\,CFSE_{low}\,to\,CFSE_{high}\,in\,na\"ive\,mice\right) \Big/ \left(ratio\,of\,CFSE_{low}\,to\,CFSE_{high}\,in\,immunized\,mice\right)\right] \times 100\%$$

2.13. *Interferon gamma (IFN-γ) production*

Days 7 after the final immunization, the splenocytes were collected from immunized mice. Splenocytes were cultured with $OVA_{257-264}$ at 37 °C for 18 h. The cell supernatants were harvested, and the IFN-γ was measured employing enzyme-linked immunosorbent assay (ELISA).

2.14. *In vivo tumor experiments for vaccines*

Female C57BL/6 mice were s.c. injected with 1×10^6 B16-OVA cells. As shown in Fig. 6A, the mice were subcutaneously immunized with Blank, OVA, OVA+CpG, PP-OVA, PP-SS-OVA and PP-SS-OVA/CpG. The tumor volumes were monitored every 2 d The mice were sacrificed when the tumor sizes achieved 1500 mm³.

Female C57BL/6 mice were i.v. injected with 5×10^5 B16-OVA cells. As shown in Fig. 6A, the mice were subcutaneously immunized with Blank, OVA, OVA+CpG, PP-OVA, PP-SS-OVA and PP-SS-OVA/CpG.

2.15. *In vivo immune combination therapy*

Subcutaneous of B16-OVA tumor model followed the above preparation method. As shown in Fig. 7A, female C57BL/6 mice were subcutaneously immunized with Blank, OVA, PP-SS-OVA and PP-SS-OVA/CpG+anti-PD-1(intravenous injection, 20 μg/mouse). The tumor volumes were monitored every two days. The mice were sacrificed when the tumor sizes achieved 1500 mm³.

Lung metastasis of B16-OVA tumor model followed the above preparation method. Female C57BL/6 mice were subcutaneously immunized with Blank, OVA, PP-SS-OVA and PP-SS-OVA/CpG+anti-PD-1(intravenous injection, 20 μg/mouse).

2.16. *Tumor-infiltrating lymphocytes analysis*

For assessment of the anti-tumor immune response after above combinational immunotherapy, tumor was digested by hyaluronidase, collagenase I, and collagenase IV at 37 °C for 1 h. Cell suspension was filtered to recover single cell suspension. The cell suspensions were incubated with anti-CD3-FITC, anti-CD4-APC, and anti-CD8-PerCP-Cy5.5 for 30 min. The cell suspensions were measured by FCM.

3. Results and discussion

3.1. *Optimized micelles to target LNs and DCs*

Vaccine carries against cancer are centered on the delivery of tumor associated antigen to lymph nodes which then initiate the cellular immune responses[26,38]. Herein, we investigated the capacity for mixed micelles to deliver cargo to distal LNs from the site of injection. As shown in Fig. 1A, cargo (DiR) distribution observed upon the IVIS spectrum showed that PP0 promoted DiR a whole-body distribution inside 6 h, while PP100 maintained DiR at Day 7 at the injection site, indicating that the interstitial migration potency of mixed micelles is
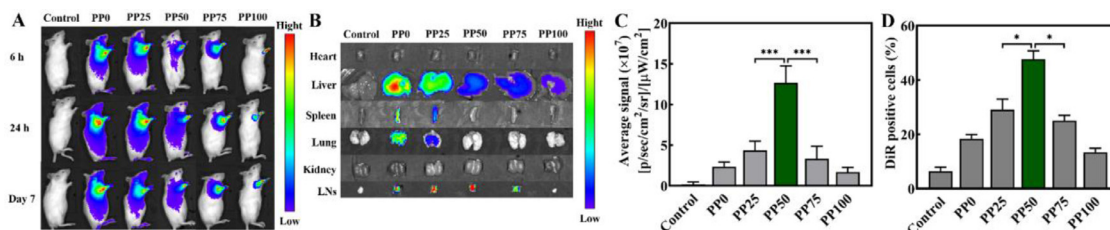

Fig. 1 – PP50 made the strongest property on inguinal LNs targeting and uptake by DCs in vivo. (A) Female BALB/c mice treated with Blank (control), DiR-loaded PP0, PP25, PP50, PP75 or PP100. Female BALB/c mice were observed by fluorescence images. (B) The heart, liver, spleen, lung, kidney and inguinal LNs were observed by fluorescence images. (C) Inguinal LNs were observed by ROI analysis at 24 h post-administration. (D) Percentages of DCs in inguinal LNs that were positive for DiR: CD11c+DCs.

inversely related to the proportion of PEI. Lower PEI accelerates the migration of mixed micelles.

Furthermore, the same conclusion can be obtained by the study of the tissues harvested from mice (Fig. 1B and 1C). The study further demonstrated that PP0 with a favorable whole-body distribution was not better to PP50 (denoted as PP) when delivering LNs. Compared to other organs, PP0 mostly accumulated in the liver. Decreasing the proportion of PEG-PCL in the mixed micelles leads to a significant reduce in the accumulation of them in the liver. However, PP75 or PP100 revealed a greatly low dispersion in all organs. PP50 was widely dispersed in LNs and rarely distributed in liver. As shown in Fig. S9 and Table S1, the diameter of all the formulations was about 20 nm as determined using DLS. But, the Zeta potential of all the formulations relied on the mol ratio of PEI-PCL/PEG-PCL, a high ratio resulting in a higher Zeta potential. We speculate that a high level PEGylation of NPs favored whole-body distribution when delivering LNs, since the PEG coating was able to reduce the interaction of NPs with glycosaminoglycans and collagen fibres in the interstitium. However, the positive charge of NPs will be caught in the interstitium before it can delivery to the LNs. Therefore, PP50 has possess strongest capacity to deliver to LNs.

The vaccines reach LNs, where tumor associated antigens are taken up by APCs, such as DCs. DCs are activated to drive the cellular immune responses[15,39]. Furthermore, the single cell suspension of lymph nodes was prepared to research the frequency of the cargo uptake by cells in LNs using FCM. As displayed in Fig. 1D, PP50 showed that the proportion of DiR positive cells is significantly higher than other control groups. The much better proportion of DiR positive cells of PP50 than PP0 or PP25 may benefit from higher positive charge on PP50,

which plays a role "agonist" to activate DCs. Consistent with previous research, cationic liposomes facilitated the antigen-specific immune response, while neutral liposomes restrained the one. The much better proportion of DiR positive cells of PP50 than PP75 or PP100 may benefit from better delivery cargo to distal LNs. These results confirmed that PP50 has the strongest capacity to deliver to LNs and the weakest capacity to enter into the systemic circulation.

3.2. Characterization of different formulations

CMC is a key character of micelles, which influences the stability of micelle framework[40]. The CMC was tested using the fluorescence spectrophotometry. Pyrene was used as a species of fluorescence probe. As shown in Fig. S8a, the CMC value was 2.35 µg/ml, indicating that the mixed micelles had good dilution stability and remained stable after subcutaneous injection. To exert cytosolic delivery of antigens effects, the NPs must be released from lysosome when it is internalized into the endo/lysosome. Therefore, the pH-sensitive delivery systems were need to possess an appropriate triggering pH value, at which a rapid NPs escape from endo/lysosomal. The pKb value of PEI-PCL was calculated acid-base titration experiments. As shown in Fig. S8b, we have demonstrated the pKb of PEI-PCL was about 5.5 which is approximate the pH value of endo/lysosome.

As shown in Fig. 2B, conjugation of OVA to the mixed micelles was measured by SDS-PAGE, and the migration of free OVA-FITC to the lower molecular weights band was found. By contrast, conjugates were not observed to migrate into the gel. It can be evaluated whether OVA have the ability to release from the mixed micelles with cytosolic levels of
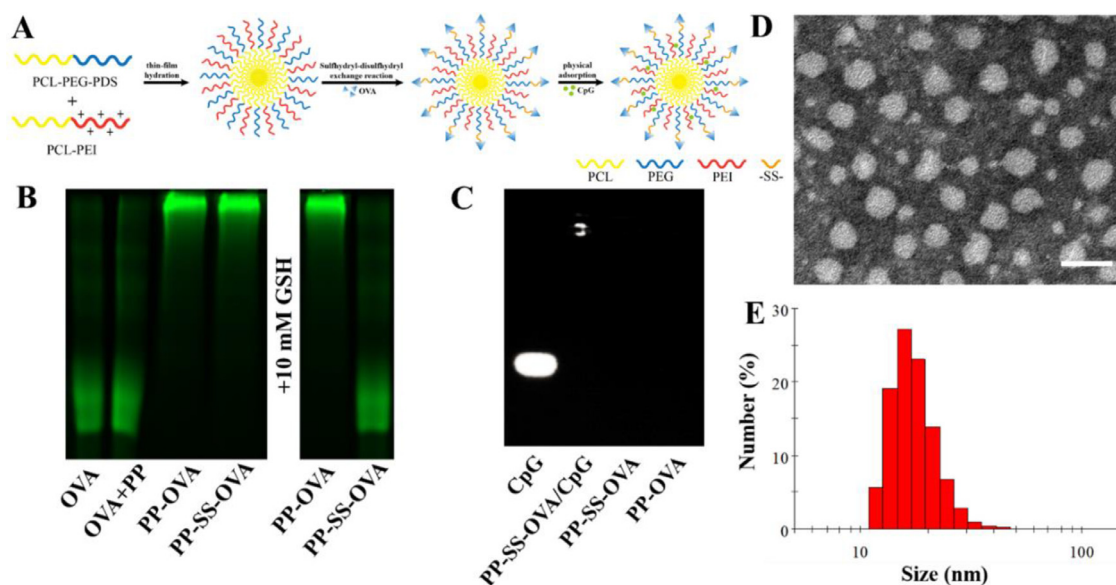

Fig. 2 – Preparation and characterization of dual-Responsive nanovaccines. (A) Schematic representation of preparation method of nanovaccines. (B) SDS-PAGE of OVA, OVA+PP, PP-OVA, and PP-SS-OVA. Incubation of PP-OVA, PP-SS-OVA with 10 mM glutathione (GSH) liberates OVA from the mixed micelles. (C) Agarose gel electrophoresis of CpG ODN$_{1826}$, PP-SS-OVA/CpG, PP-SS-OVA and PP-OVA. (D) TEM image of PP-SS-OVA/CpG NPs, Scale bar =50 nm. (E) The size distribution of PP-SS-OVA/CpG NPs measured by DLS. (For interpretation of the references to colour in this figure legend, the reader is referred to the web version of this article.)

glutathione (10 mM) by nonreducing SDS-PAGE. The disulfide bonds linked OVA to the mixed micelles were degraded in the presence of glutathione, indicating that PP-SS-OVA was able to release OVA in the DC cytosol, facilitating efficiency of antigen cross-presentation. By contrast, the amide bond between OVA and mixed micelles were not degraded by glutathione. The conjugation efficiency assayed by a bicinchoninic (BCA) protein was about 95%. As shown in Fig. 2C, the migration of the free CpG to the cathode blocked by the mixed micelles through gel retardation assays, suggesting that CpG was completely complexed to mixed micelles. As shown in Fig. 2D and 2E, the diameter of PP-SS-OVA/CpG NPs about 20–30 nm was measured using DLS. The same results can be observed by TEM, suggesting that all the nanovaccines were stable and uniform. As shown in Fig. S9 and Table S1, the size distribution of all the mixed micelles (PP0, PP25, PP50, PP75 and PP100) was about 25 nm as determined using a DLS. The Zeta potential of all the mixed micelles (PP0, PP25, PP50, PP75 and PP100) is −17, 13, 32, 36 and 46 mV, respectively. Co-loading of OVA and CpG into the mixed micelles did not visibly influence the size of all the nanovaccines, based on the DLS.

3.3. Cellular cytotoxicity and cellular uptake

DCs are a crucial APCs and as a key role in activating of antigen specific T cells [39,41,42]. As shown in Fig. S10A and S10B, we found that neither PP-SS-OVA nor PP-OVA has no obvious cytotoxic effects on BMDCs through MTT experiment. As shown in Fig. S11a and b, PP-OVA or PP-SS-OVA could enhance remarkable antigen cross-presentation and DC maturation. The OVA was chosen to the following assays.

The cellular uptake of OVA, PP-OVA, and PP-SS-OVA were evaluated by FCM and CLSM. BMDCs were culture with Blank, OVA, PP-OVA, or PP-SS-OVA for 4 h. As shown in Fig. 3A, compared to the OVA, both PP-OVA and PP-SS-OVA can promote the uptake of BMDCs. As shown in Fig. 3B, the same result was also determined using FCM, indicating that mixed micelles could boost the intracellular antigen delivery. We speculate that the enhanced uptake profit from higher zeta potential, showing the significance of positive charge for NPs uptake.

We used CLSM to further investigate the intracellular localization of PP-OVA or PP-SS-OVA in BMDCs. BMDCs was cultured with PP-OVA or PP-SS-OVA NPs at 37 °C for 1 h,
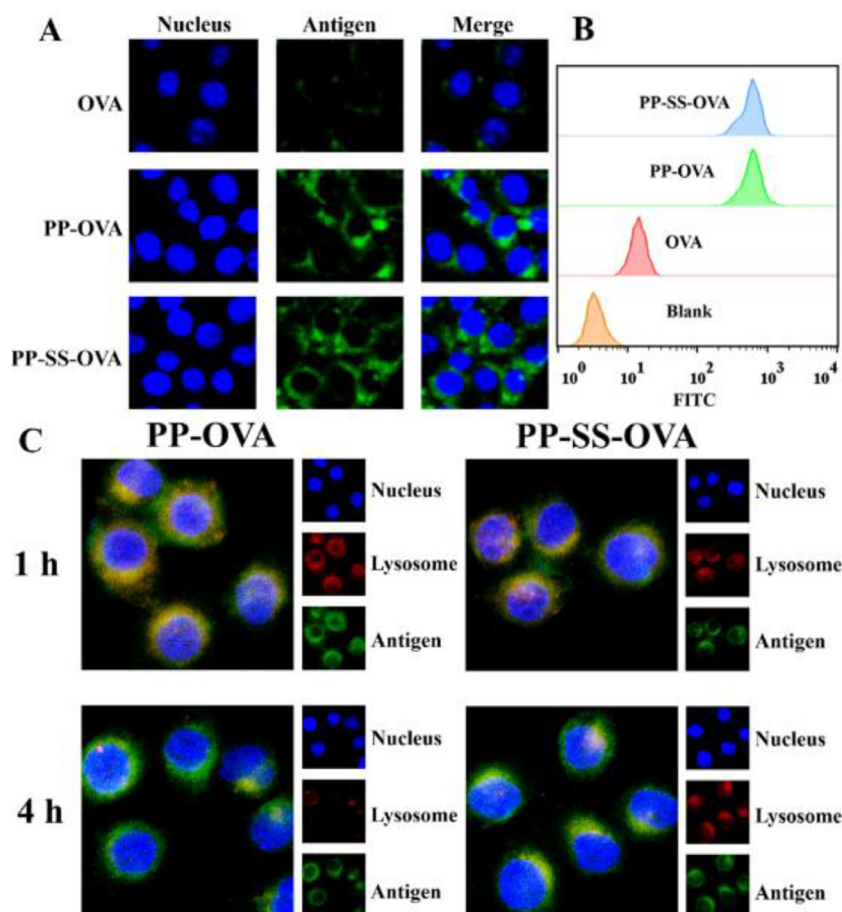

Fig. 3 – In vitro NPs uptake by BMDCs. (A) OVA, PP-OVA and PP-SS-OVA were treated to BMDCs for 4 h, the signals were observed by CLSM. (B) Uptake of OVA, PP-OVA and PP-SS-OVA by BMDCs as determined using FCM. (C) Intracellular OVA release of PP-OVA and PP-SS-OVA were observed by CLSM. The blue, green, and red shows the nuclei, OVA, and endo/lysosomes, respectively. (For interpretation of the references to colour in this figure legend, the reader is referred to the web version of this article.)
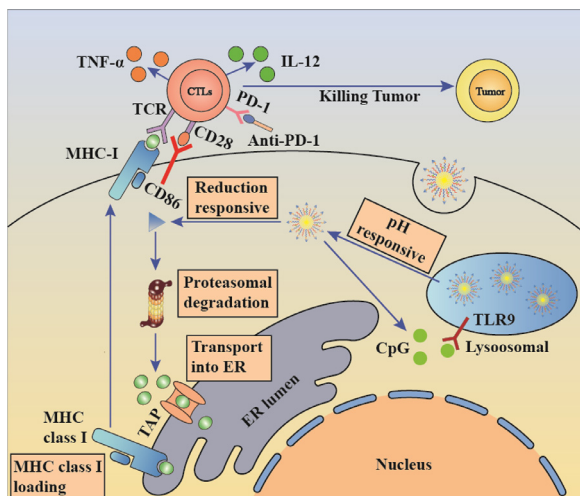
Scheme 1 – PP-SS-OVA/CpG could improve MHC I cross-presentation via promoting cytosolic antigen release and then the combination of PP-SS-OVA/CpG and anti-PD1 therapy elicits effective cellular immune response killing the tumor.

as shown in Fig. 3C, a yellow fluorescence occupied most of the merged images, indicating that the NPs resided in lysosome. BMDCs was cultured with PP-OVA or PP-SS-OVA NPs at 37 °C for 4 h, as shown in Fig. 3C, which showed the isolation of green and red fluorescence, suggesting that NPs could effectively escape from the lysosome. Combined with the results above, we speculate that NPs was protonated under endo/lysosomal acidic conditions and stimulates the endo/lysosomal escape of it via a "proton sponge" effect (Scheme 1).

3.4. Efficiency of cross-presentation of NPs-conjugated antigens is conjugation chemistry-dependent

An effective nanovaccine can induce antigen-specific cytotoxicity (CD8^{+}) T lymphocytes [42,43]. The activity of the CTLs is decided by efficiency of antigen MHC-I cross-presentation. To study the efficiency of antigen MHC-I cross-presentation following NP-conjugation antigen uptake, we employed the anti-SIINFEKL/H-2K[b]PE that identify MHC-I complexes combined with OVA$_{257-264[30]}$. As shown in Fig. 4E, PP-SS-OVA$_{257-264}$ were successfully captured by BMDCs, the differences between OVA$_{257-264}$ and OVA conjugated by disulfide bond were inappreciable. However, when OVA was conjugated by non-reducible amide bond, antigen MHC-I cross-presentation was remarkably inhibited [44]. The PP-OVA degradation may need an oxidative process or a proteolytic process before OVA can be released [45]. These results indicated that the reduction-sensitive release of antigen from the mixed micelles appears much earlier than the other step of the mixed micelles.

3.5. Nanoparticle carriers promote antigen cross-presentation, BMDCs maturation and cytokine secretion

Exogenous antigens were captured by DCs to elicit following immune responses via interaction with CTLs [39,46]. The

high expression of CD80 and CD86 as well as antigen peptide-MHC-I complexes would be triggers for priming CD8^{+} T-cells. The percentage of CD11c^{+}CD86^{+}CD80^{+}DCs and CD11c^{+}SIINFEKL^{+}DCs were separately analyzed by FCM. As shown in Fig. 4A, and 4B, the antigen MHC-I cross-presentation efficiency of PP-SS-OVA was 1.6 times higher than that of PP-OVA. Moreover, antigen MHC-I cross-presentation efficiency of PP-SS-OVA was 5.1 times higher than that of free OVA. As shown in Fig. 4C and 4D, the expression of CD80 and CD86 of PP-SS-OVA was 1.3 times higher than that of PP-OVA and was 1.8 times higher than that of free OVA, indicating that the OVA conjugated by disulfide bond could effectively facilitate antigen MHC-I cross-presentation and the DC maturation. When disulfide bond-NPs were degraded under a cytosol reductive-sensitive environment, which induced much more remarkable MHC-I cross-presentation and DC maturation. Furthermore, the antigen MHC-I cross-presentation efficiency of PP-SS-OVA/CpG was 1.6 times higher than that of PP-SS-OVA and was 4.3 times higher than that of free OVA+CpG; the expression of co-stimulatory (CD80, CD86) molecules of PP-SS-OVA/CpG was 30% higher than that of PP-SS-OVA and was 50% higher than that of free OVA+CpG, suggesting that incorporation of CpG ODN into the PP-SS-OVA system could notably raise the immunogenicity of antigens and then elicit CTL responses.

The BMDC maturation was proved by cytokine production. It has been reported that IL-12p70 and TNF-α are an indispensable cytokine for priming cellular immune responses [47]. As shown in Fig. 4F and 4G, compared with PP-OVA or OVA, the PP-SS-OVA could induce much more production of IL-12p70 and TNF-α. This could owe to the disulfide bond have the property of the cytosol reduction-sensitive. PP-SS-OVA/CpG could elicit greatest secretion of IL-12p70 and TNF-α than other groups. In summary, it is proved that reduction-sensitive bond is considered to be essential for the effectiveness of tumor vaccine, meanwhile, incorporation of CpG ODN into the PP-SS-OVA system could significantly elicit antigen MHC-I cross-presentation and DC maturation.

3.6. Nanoparticle carriers enhance BMDC maturation and cytokine secretion in vivo

We investigated antigen cross-presentation and DC maturation on day 3 after immunization. As shown in Fig. 5A and 5B, the expression of CD80 and CD86 of PP-SS-OVA was 30% higher than that of PP-OVA and was 90% higher than that of free OVA, indicating that the OVA conjugated by disulfide bond could effectively promote the DC maturation in vivo. When administered in vivo, the expression of co-stimulatory (CD80, CD86) molecules of PP-SS-OVA/CpG was 80% higher than that of PP-SS-OVA and was 2.3 times higher than that of free OVA+CpG, suggesting that incorporation of CpG ODN into the PP-SS-OVA system could notably raise the DC maturation and further initiate antigen-specificity immune responses.

Interferon gamma (IFN-γ) is an important marker of CTLs in the immunotherapy [18,47]. To assess whether these formulations of vaccine could boost T-cell immune responses
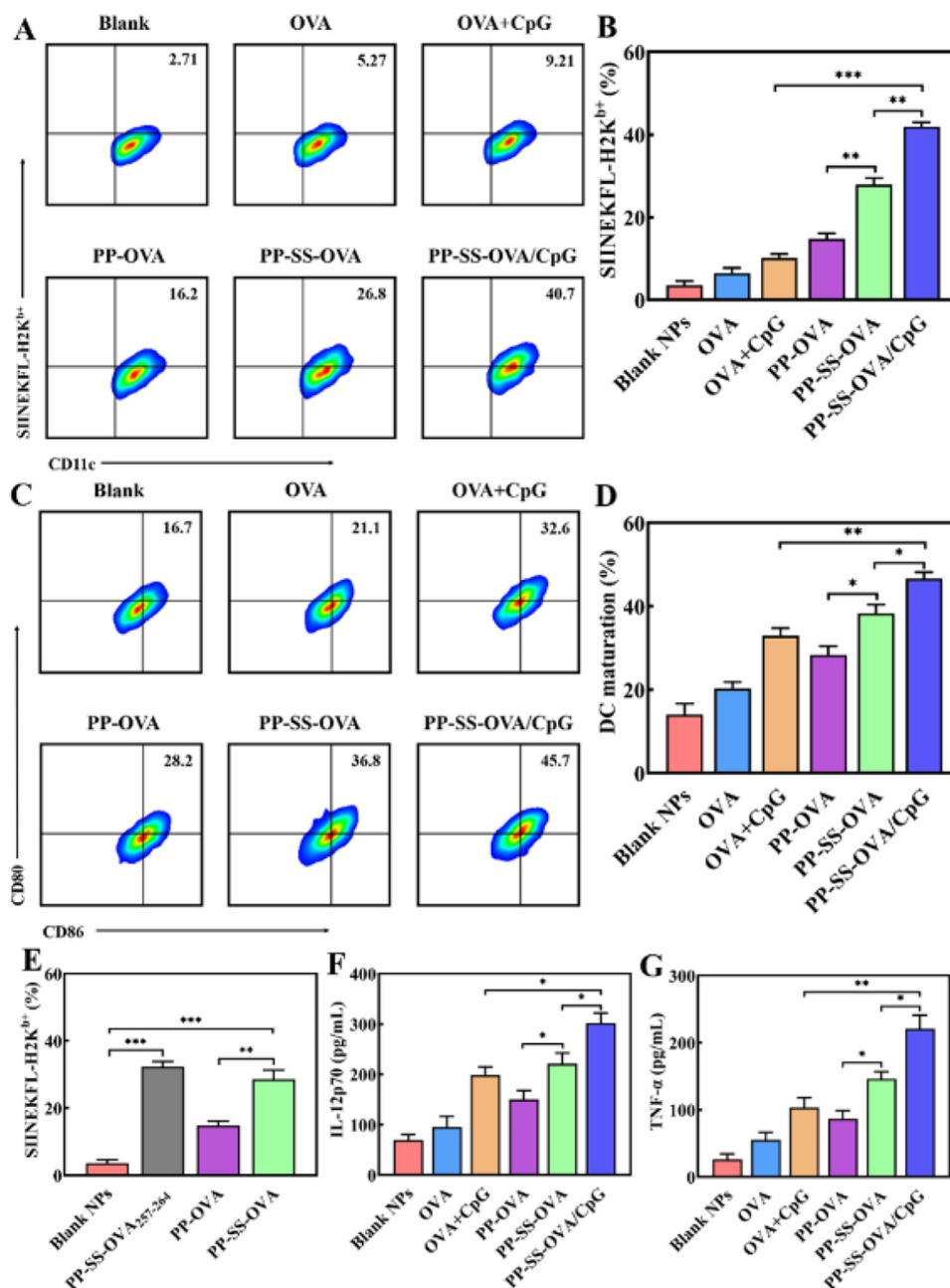
Fig. 4 – Disulfide bond conjugates promote MHC-I antigen cross-presentation and DCs maturation in vitro. (A&B) Expression of CD11c$^+$SIINFEKL$^+$DCs was analyzed using FCM. (C&D) Expression of CD11c$^+$CD86$^+$CD80$^+$DCs was analyzed using FCM. (E) Expression of CD11c$^+$SIINFEKL$^+$DCs was analyzed using FCM. (F&G) The production of IL-12p70 and TNF-α cytokines were analyzed using ELISA kits.

in vivo. As shown in Fig. 5E, the generation of IFN-γ^+ CTLs of PP-SS-OVA was 50% higher than that of PP-OVA and was 4.9 times higher than that of free OVA, suggesting that OVA conjugated by disulfide bond is necessary in generation of IFN-γ^+. In addition, compared to free OVA+CpG or PP-SS-OVA, PP-SS-OVA/CpG could elicit the highest level of IFN-γ^+ CTLs, suggesting that incorporation of CpG-ODN into the PP-SS-OVA system could trigger one more IFN-γ^+ CTLs generation than unformulated adjuvant. As shown in Fig. S14, there was no obvious toxicity in the heart, liver, spleen, lung and kidney. In

summary, these results confirmed PP-SS-OVA/CpG NPs could elicit in vivo antigen cross-presentation and DC maturation.

3.7.   CTLs assay in vivo

CTLs are a crucial role in inhibiting growth of tumor cells or the prevention of cancer recurrence [21,48]. To evaluate whether the mixed micelles can trigger robust cellular immunity, we measured the specific lysis of PP-SS-OVA/CpG NPs. As shown in Fig. 5C and 5D, free OVA or PBS did not
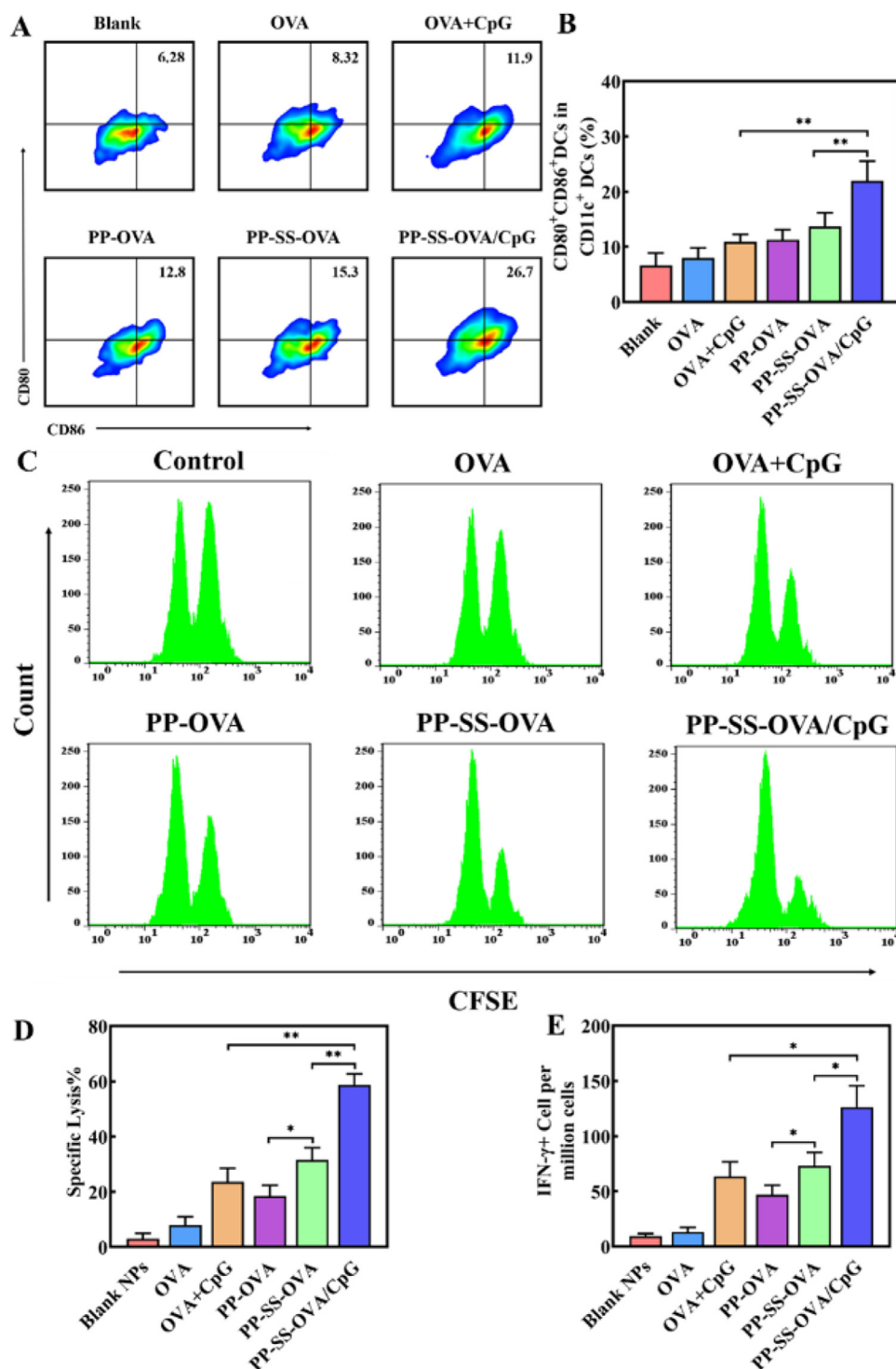
Fig. 5 – *In vivo* CTL response and DC maturation after vaccination. (A&B) Expression of CD11c$^+$CD86$^+$CD80$^+$DCs was measured by FCM. (C&D) CTL activity after vaccination in vivo. (E) IFN-γ was measured by ELISA. (For interpretation of the references to colour in this figure legend, the reader is referred to the web version of this article.)

exhibit OVA$_{257-264}$-specific CTLs response. The free OVA+CpG or PP-OVA, and approximately 20% OVA$_{257-264}$ pulsed target cells were killed. In contrast, the mice immunized with PP-SS-OVA was able to kill about 35% OVA$_{257-264}$-pulsed target cells, suggesting that OVA conjugated by disulfide bond is a crucial role in generation of CTLs. The PP-SS-OVA/CpG NPs was able

to kill about 60% OVA$_{257-264}$-pulsed target cells, implying the PP-SS-OVA/CpG NPs induce an effective in vivo OVA$_{257-264}$-specific CTLs response compared with other groups. In the present work, PP-OVA or PP-SS-OVA could produce moderate CTL response and tumor inhibitory activity, indicating that the NPs may activate DCs moderately. This is similar to
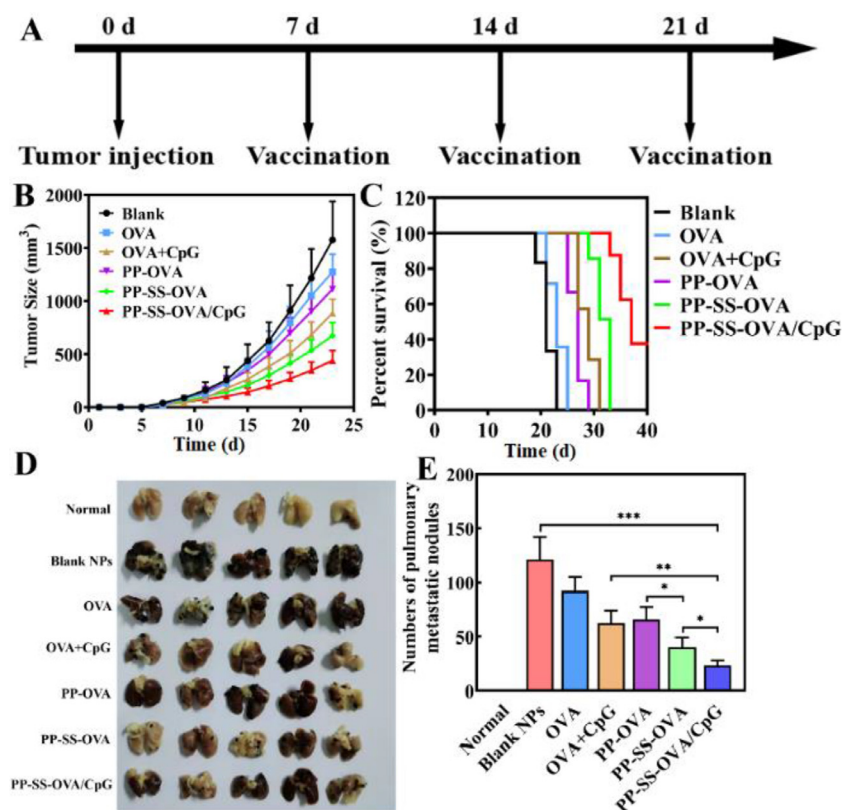
Fig. 6 – Anti-tumor activity of different nanovaccine in vivo. (A) Scheme of inhibition tumor and metastasis experiment. (B) Variation in tumor volume of mice. (C) Survival curves of mice for various formulations. (D) Lungs were harvested for imaging. (E) Numbers of tumor nodules were counted manually in the lung.

previous reports that cationic NPs are not only a carrier but also an effective vaccine adjuvant to trigger immune response.

3.8. Nanoparticle carriers enhance antitumor activity

As shown in Fig. 6A, the mice were subcutaneously injected on Day 0 with B16-OVA cells. The mice were subcutaneously injected with PBS, OVA, OVA+CpG, PP-OVA, PP-SS-OVA and PP-SS-OVA/CpG separately on Day 7, 14 and 21. As shown in Fig. 6B and S12, compared to PP-OVA and OVA alone, immunization with PP-SS-OVA NPs could partially suppress the tumor growth. Surprisingly, CpG ODN was integrated into PP-SS-OVA, the obtained PP-SS-OVA/CpG NPs had the most potent tumor growth inhibitory effect. As shown in Fig. 6C, the survival of mice immunized with the PP-SS-OVA was prolonged the 15% than that of PP-OVA and was prolonged the 30% than that of free OVA. The survival with the PP-SS-OVA/CpG group was prolonged the 50% than that of other ones, indicating that PP-SS-OVA/CpG group can induce effective cellular immune response to suppress tumor growth. It is critical for CpG ODN introducing into PP-SS-OVA that can maximize inducing immunogenicity to enhance the cellular immune response. This result is similar to CTLs assay in vivo, indicating that codelivery of OVA and CpG ODN in nanovaccine forms could elicit strong the cellular immune response superior to vaccination by delivery of OVA.

Whether PP-SS-OVA/CpG NPs could inhibit B16-OVA metastasis was another critical issue. The mice were injected via tail vein on day 0 with B16-OVA melanoma cells. The mice were subcutaneously injected on days 7, 14 and 21 with formulations PBS, OVA, OVA+CpG, PP-OVA, PP-SS-OVA and PP-SS-OVA/CpG separately. As shown in Fig. 6D, PP-SS-OVA/CpG NPs shown the most potent tumor metastasis inhibition, exhibiting the least lung metastatic nodules. As shown in Fig. 6E, the numbers of lung metastatic nodules of PP-OVA or OVA was 1.7 or 2.3 times higher than the numbers of lung metastatic nodules of PP-SS-OVA, indicating that OVA conjugated by disulfide bond could notably enhance the antigen cross-presentation and further initiate CTL responses. The numbers of lung metastatic nodules of PP-SS-OVA or OVA+CpG was 1.8 or 2.7 times higher than that of PP-SS-OVA/CpG, indicating that the PP-SS-OVA/CpG NPs could produce CTL response and tumor inhibitory activity.

3.9. Combination immunotherapy enhance antitumor activity

The PD-1 blockade in combination with other antitumor therapy strategies have provided tremendous potential in cancer treatment in recent years [4,49]. As shown in Fig. 7A, the therapeutic effect of anti-PD-1 blockade in combination with PP-SS-OVA/CpG NPs strategy was also assessed. As shown in Fig. 7B, C and S13, PP-SS-OVA/CpG group or anti-
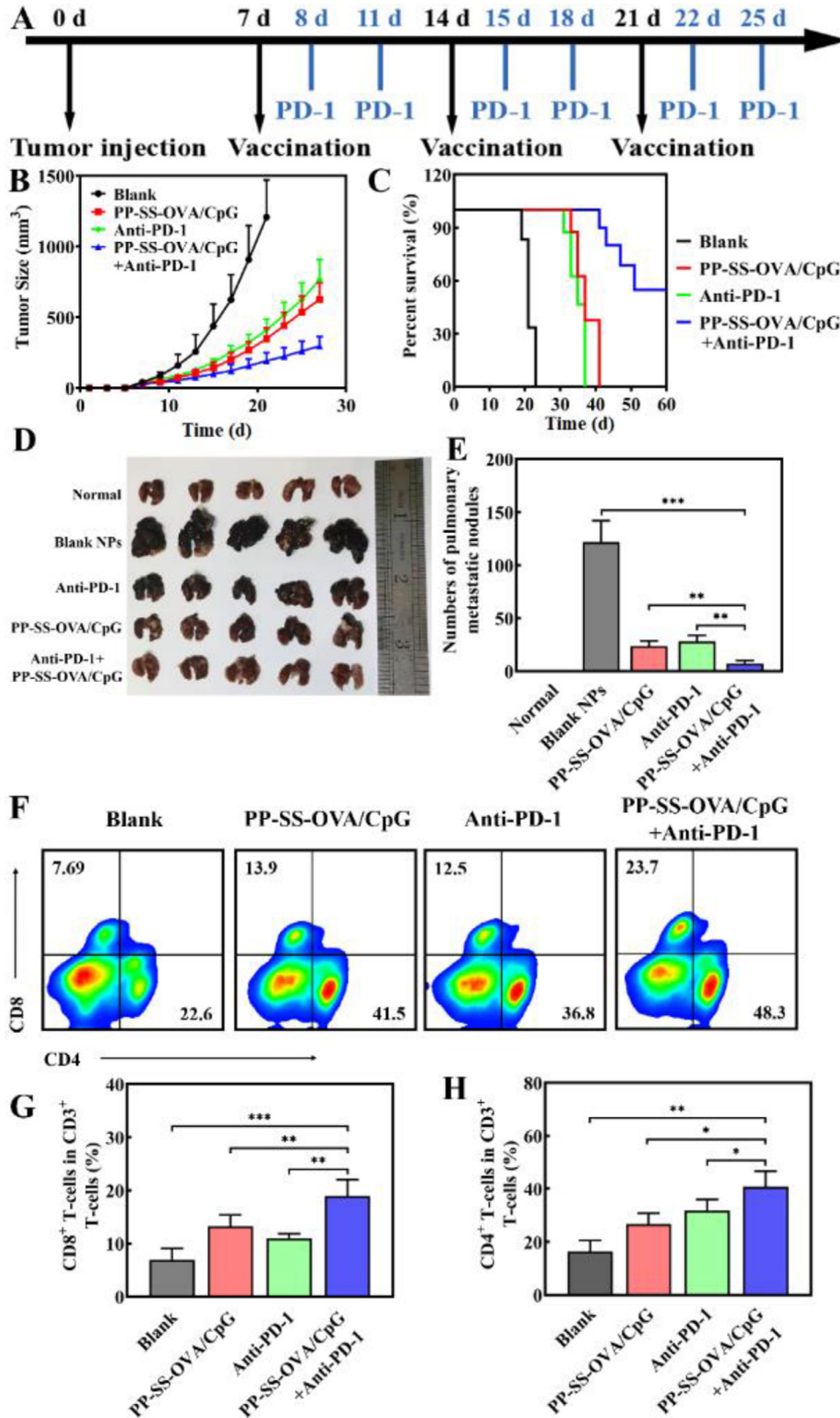
Fig. 7 – Combination of PP-SS-OVA/CpG with anti-PD-1 for immunotherapy could elicit stronger antitumor activity in vivo. (A) Scheme of inhibition tumor and metastasis experiment for combination of PP-SS-OVA/CpG with anti-PD-1. (B) Variation in tumor growth curves. (C) Survival curves of mice. (D) Lungs were harvested for imaging. (E) Numbers of tumor nodules were counted manually in the lung. (F-H) Expression of $CD3^+CD8^+$ and $CD3^+CD4^+$ T-cells were analyzed using FCM in tumors.

PD-1 single therapy could partially inhibit tumor. Interestingly, mice immunized with a combined treatment of PP-SS-OVA/CpG NPs and anti-PD-1, the tumor volume was potently suppressed and the mice survival rate was increased to 50% within 60 d As shown in Fig. 7D, the PP-SS-OVA/CpG NPs+anti-PD-1 exhibited the most potent tumor metastasis inhibition. As shown in Fig. 7E, numbers of lung metastatic nodules of PP-SS-OVA/CpG or anti-PD-1 was 3.3 times or 4.1 times higher than that of PP-SS-OVA/CpG+anti-PD-1, indicating that the anti-PD-1 could enhance synergistically antitumor activity in the combinational immunotherapy. As shown in Fig. S15, no perceptible body weight decrease was observed with PP-SS-OVA/CpG group, indicating the no obvious toxicity of NPs to the treated mice.

3.10. Tumor-infiltrating lymphocytes analysis

To assess whether combination therapy could trigger antitumor response. It is known that anti-PD-1 promotes the infiltration of tumors, leading to cellular immune response [4,5,49]. Hence, the tumors were harvested on day 13. The tumor infiltrating T-cells were analyzed by FCM. As shown in Fig. 7F-7H and S16, when combined PP-SS-OVA/CpG NPs with anti-PD-1 therapy, the percentages of tumor-infiltrating $CD3^+CD4^+$ and $CD3^+CD8^+$ T-cells among $CD3^+$T cells within the tumors were remarkably enhanced. In contrast, $CD8^+$ and $CD4^+$T cells were not adequately infiltrated into tumors by PP-SS-OVA/CPG or anti-PD-1 simple therapy.

In summary, the theories of combinational immunotherapy strategy may be interpreted as follows: (1) The PP-SS-OVA/CpG NPs were able to induce cellular immunity; mixed micelles were able to promote cargo delivery and antigen MHC-I cross-presentation; the CpG ODN could facilitate the immunogenicity [25,50,51]. (2) Anti-PD-1 was able to potently enhance CTL infiltration into tumors, enhancing antitumor activity in the combinational immunotherapy [34,49].

4.   Conclusions

In summary, the mixed micelles were prepared as a multifunctional carrier for co-delivering OVA and CpG ODN. The mixed micelles were optimized by incorporating the advantages of both cationic PEI-PCL and anionic PEG-PCL, which can deliver to LNs and boost antigens taken up by DCs. In this system, antigens were conjugated to the surface of NPs by disulfide bonds increasing the accumulation of antigens on LNs, potentiating the cytosol delivery of antigens which would induce efficient antigen cross-presentation in DCs. CpG ODN was introduced into PP-SS-OVA by simple mixing, the obtained PP-SS-OVA/CpG NPs further promoted antigen immunogenicity initiating potent anti-tumor immunity. The PP-SS-OVA/CpG+anti-PD-1 could not only trigger strong therapeutic efficacy, but also to potently control lung metastasis tumor. This work prominent that we conjugated antigen to NPs surface by the disulfide bond for cytosol delivery of antigens, owing to more intelligent design of carriers. Our study offers a new point of a rational delivery design of antigens to induce cellular immune response.

Supplementary materials

REFERENCES

[1] Couzin-Frankel J. Breakthrough of the year 2013 cancer immunotherapy. Science 2013;342(6165):1432–3.

[2] Farkona S, Diamandis EP, Blasutig IM. Cancer immunotherapy: the beginning of the end of cancer. BMC Med 2016;14(1):1–18.

[3] Banchereau J, Palucka K. Immunotherapy: cancer vaccines on the move. Nat Rev Clin Oncol 2018;15(1):9–10.

[4] Postow MA, Callahan MK, Wolchok JD. Immune Checkpoint blockade in Cancer Therapy. J Clin Oncol 2015;33(17): 1974–1982.

[5] Topalian S, Drake C, Pardoll D. Immune checkpoint blockade: a common denominator approach to cancer therapy. Cancer Cell 2015;27(4):450–61.

[6] Restifo NP, Dudley ME, Rosenberg SA. Adoptive immunotherapy for cancer: harnessing the T cell response. Nat Rev Immunol 2012;12(4):269–81.

[7] Guimaraes P, Gaglione S, Sewastianik T, Carrasco RD, Langer R, Mitchell MJ. Nanoparticles for immune cytokine TRAIL-based cancer therapy. ACS Nano 2018;12(2):912–31.

[8] Kaminskas LM, Porter C. Targeting the lymphatics using dendritic polymers (dendrimers). Adv Drug Deliv Rev 2011;63(10–11):890–900.

[9] Kang J, Demaria S, Formenti S. Current clinical trials testing the combination of immunotherapy with radiotherapy. J Immunother Cancer 2016;4(5):43–63.

[10] Moon JJ, Suh H, Yadava A, Irvine DJ, Liu Haipeng, Huang Bonnie, et al. Interbilayer-crosslinked multilamellar vesicles as synthetic vaccines for potent humoral and cellular immune responses. Nat Mater 2011;10(1):243–51.

[11] Burg S, Arens R, Ossendorp F, Hall TV, Melief C. Vaccines for established cancer: overcoming the challenges posed by immune evasion. Nat Rev Cancer 2016;16(4):219–33.

[12] Schwendeman Anna, Bahjat Keith S, Moon James J, et al. Designer vaccine nanodiscs for personalized cancer immunotherapy. Nat Mater 2017;16(4):489–96.

[13] Shi G, Zhang C, Xu R, Niu J, Song H, Zhang X, et al. Enhanced antitumor immunity by targeting dendritic cells with tumor cell lysate-loaded chitosan nanoparticles vaccine. Biomaterials 2017;113:191–202.

[14] An M, Meng L, Xi J, Liu H. Silica nanoparticle as a lymph node targeting platform for vaccine delivery. ACS Appl Mater Interfaces 2017;9(28):34–47.

[15] Jiang H, Wang Q, Sun X. Lymph node targeting strategies to improve vaccination efficacy. J Controlled Release 2017;267(10):47–56.

[16] Kapadia CH, Perry JL, Tian S, Luft JC, Desimone JM. Nanoparticulate immunotherapy for cancer. J Controlled Release 2015;21(9):167–80.

[17] Villadangos JA, Schnorrer P. Intrinsic and cooperative antigen-presenting functions of dendritic-cell subsets in vivo. Nat Rev Immunol 2007;7(7):543–55.

[18] Zhu G, Zhang F, Ni Q, Niu G, Chen X. Efficient nanovaccine delivery in cancer immunotherapy. ACS Nano 2017;11(3):2387–92.

[19] Manolova V, Flace A, Bauer M, Schwarz K, Saudan P, Bachmann M, et al. Nanoparticles target distinct dendritic cell populations according to their size. Eur J Immunol 2010;38(5):1404–13.

[20] Niikura K, Matsunaga T, Suzuki T, Kobayashi S, Sawa H. Gold nanoparticles as a vaccine platform: influence of size and shape on immunological responses in vitro and in vivo. ACS Nano 2013;7(5):3926–38.

[21] Xu Z, Ramishetti S, Tseng YC, Guo S, Huang L. Multifunctional nanoparticles co-delivering Trp2 peptide and CpG adjuvant induce potent cytotoxic T-lymphocyte response against melanoma and its lung metastasis. J Controlled Release 2013;172(1):259–65.

[22] Zhan X, Tran KK, Shen H. Effect of the Poly(ethylene glycol) (PEG) density on the access and uptake of particles by antigen-presenting cells (APCs) after Subcutaneous Administration. Mol Pharm 2012;9(12):3442–51.

[23] Trevaskis NL, Kaminskas LM, Porter C. From sewer to saviour-targeting the lymphatic system to promote drug exposure and activity. Nat Rev Drug Discovery 2015;14(11):781–803.

[24] Zhuang Y, Ma Y, Wang C, Hai L, Yan C, Zhang Y, et al. PEGylated cationic liposomes robustly augment vaccine-induced immune responses: role of lymphatic trafficking and biodistribution. J Controlled Release 2012;159(1):135–42.

[25] Toshiki Sekiya, Junya Yamagishi, John Henry, et al. PEGylation of a TLR2-agonist-based vaccine delivery system improves antigen trafficking and the magnitude of ensuing antibody and CD8$^+$ T cell responses. Biomaterials 2017;137:61–72.

[26] Qian Y, Jin H, Qiao S, Dai Y, Huang C, Lu L, et al. Targeting dendritic cells in lymph node with an antigen peptide-based nanovaccine for cancer immunotherapy. Biomaterials 2016;98:171–83.

[27] Lv H, Zhang S, Wang B, Cui S, Yan J. Toxicity of cationic lipids and cationic polymers in gene delivery. J Controlled Release 2006;114(1):100–9.

[28] Meng F, Hennink WE, Zhong Z. Reduction-sensitive polymers and bioconjugates for biomedical applications. Biomaterials 2009;30(12):2180–98.

[29] Li H, Jiang H, Zhao M, Yao F, Sun X. Intracellular redox potential-responsive micelles based on polyethylenimine-cystamine-poly(epsilon-caprolactone) block copolymer for enhanced miR-34a delivery. Polym Chem 2015;6(11):1952–60.

[30] Hirosue S, Kourtis C, Vlies A, Hubbell JA, Swartz MA. Antigen delivery to dendritic cells by poly(propylene sulfide) nanoparticles with disulfide conjugated peptides: cross-presentation and T cell activation. Vaccine 2010;28(50):7897–906.

[31] Hong S, Ackerman Anne L, Cody Virginia, Alessandra Giodini, Hinson Ella R, et al. Enhanced and prolonged cross-presentation following endosomal escape of exogenous antigens encapsulated in biodegradable nanoparticles. Immunology 2006;117(1):78–88.

[32] Zeng Q, Li H, Jiang H, Yu J, Wang Y, Ke H, et al. Tailoring polymeric hybrid micelles with lymph node targeting ability to improve the potency of cancer vaccines. Biomaterials 2017;122:105–13.

[33] Wang J, Fang X, Liang W. Pegylated phospholipid micelles induce endoplasmic reticulum-dependent apoptosis of cancer cells but not normal cells. ACS Nano 2012;6(6):5018–30.

[34] Xu J, Wang H, Xu L, Chao Y, Wang C, Han X, et al. Nanovaccine based on a protein-delivering dendrimer for effective antigen cross-presentation and cancer immunotherapy. Biomaterials 2019;207:1–9.

[35] Armando S, Evan A, Karen Y, Swartza M, Hubbell J. Tunable T cell immunity towards a protein antigen using polymersomes vs. solid-core nanoparticles. Biomaterials 2013;34(17):4339–46.

[36] Van AJ, O'Neil CP, Hasegawa U, Hammond N, Hubbell JA. Synthesis of pyridyl disulfide-functionalized nanoparticles for conjugating thiol-containing small molecules, peptides, and proteins. Bioconjug Chem 2010;21(4):653–62.

[37] Vallecillo MS, Gamboa GU, Palma SD, Harman MF, Chiodetti AL, Morón G, et al. Adjuvant activity of CpG-ODN formulated as a liquid crystal. Biomaterials 2014;35(8):2529–42.

[38] Rock KL, York IA, Goldberg AL. Post-proteasomal antigen processing for major histocompatibility complex class I presentation. Nat Immunol 2004;5(7):670–7.

[39] Joffre OP, Segura E, Savina A, Amigorena S. Cross-presentation by dendritic cells. Nat Rev Immunol 2012;12(8):557–69.

[40] Qiu L, Qiao M, Chen Q, Tian C, Long M, Wang M, et al. Enhanced effect of pH-sensitive mixed copolymer micelles for overcoming multidrug resistance of doxorubicin. Biomaterials 2014;35(37):9877–87.

[41] Luo M, Wang H, Wang Z, Cai H, Gao J. A STING-activating nanovaccine for cancer immunotherapy. Nat Nanotechnol 2017;12(7):648–54.

[42] Scott EA, Stano A, Gillard M, Maio-Liu AC, Swartz MA, Hubbell JA. Dendritic cell activation and T cell priming with adjuvant- and antigen-loaded oxidation-sensitive polymersomes. Biomaterials 2012;33(26):6211–19.

[43] Palucka K, Banchereau J. Cancer immunotherapy via dendritic cells. Nat Rev Cancer 2012;12(4):265–77.

[44] Norbury CC, Chambers BJ, Prescott AR, Ljunggren HG, Watts C. Constitutive macropinocytosis allows TAP-dependent major histocompatibility complex class I presentation of exogenous soluble antigen by bone marrow-derived dendritic cells. Eur J Immunol 2010;27(1):280–8.

[45] Rehor A, Hubbell JA, Tirelli N. Oxidation-sensitive polymeric nanoparticles. Langm ACS J Surf Colloids 2005;21(1):411–17.

[46] Liu L, Cao F, Liu X, Wang H, Zhang C, Sun H, et al. Hyaluronic acid-modified cationic lipid-PLGA hybrid nanoparticles as a nanovaccine induce robust humoral and cellular immune responses. ACS Appl Mater Interfaces 2016;8(19):11969–79.

[47] Nastala CL, Edington HD, Mckinney TG, Tahara H, Storkus WJ. Recombinant IL-12 administration induces tumor regression in association with IFN-gamma production. J Immunol 1994;153(4):1697–706.

[48] Melief Cornelis JM, Burg Sjoerd HVan Der, FO Rene EMToes, Offringa Rienk. Effective therapeutic anticancer vaccines based on precision guiding of cytolytic T lymphocytes. Immunol Rev 2010;188(1):177–82.

[49] Pardoll DM. The blockade of immune checkpoints in cancer immunotherapy. Nat Rev Cancer 2012;12(4):252–64.

[50] Krieg AM. Therapeutic potential of Toll-like receptor 9 activation. Nat Rev Drug Discovery 2006;5(6):471–84.

[51] Zhang W, An M, Xi J, Liu H. Targeting CpG Adjuvant to lymph node via dextran conjugate enhances anti-tumor immunotherapy. Bioconjug Chem 2017;28(7):1993–2000.